Sensors & Actuators: B. Chemical 358 (2022) 131510

Contents lists available at ScienceDirect

Sensors and Actuators: B. Chemical

journal homepage: www.elsevier.com/locate/snb

Calibration-free mid-infrared exhaled breath sensor based on BF-QEPAS for real-time ammonia measurements at ppb level

Biao Li [a,b], Chaofan Feng [a,b], Hongpeng Wu [a,b], Suotang Jia [a,b], Lei Dong [a,b,*]

[a] State Key Laboratory of Quantum Optics and Quantum Optics Devices, Institute of Laser Spectroscopy, Shanxi University, Taiyuan 030006, China
[b] Collaborative Innovation Center of Extreme Optics, Shanxi University, Taiyuan 030006, China

ARTICLE INFO

Keywords:
Beat frequency
Photoacoustic spectroscopy
Calibration-free breath sensor
Quantum cascade lasers
NH_3 detection

ABSTRACT

Breath analysis, compared with blood analysis, can enable real-time non-invasive diagnostics through quantification of exhaled biomarkers. Here, we demonstrate, for the first time, a calibration-free mid-infrared (MIR) exhaled breath sensor for real-time ammonia measurements at ppb-level, which can be used for the non-invasive diagnosis of liver and kidney diseases. The exhaled breath sensor employs a 10.359-μm MIR quantum cascade laser (QCL) to target a strong NH_3 absorption line and adopts the beat-frequency quartz-enhanced photoacoustic technique (BF-QEPAS) to remove the requirements of calibration process and wavelength locking in the conventional QEPAS technique. By studying the adsorption-desorption effect and optimizing the modulation depth and modulation frequency of the sensor system, a detection limit of 9.5 ppb is achieved at an integration time of 3 ms. The ammonia content exhaled by 8 healthy volunteers is recorded and the real-time measurement results are analyzed. Compared with conventional QEPAS sensors, the proposed BF-QEPAS-based sensor offers higher sensitivity, faster response time, as well as no need for calibration and wavelength locking.

1. Introduction

Variations in ammonia (NH_3) levels in human body are related to the dysfunction of the liver and kidneys since ammonia is mainly excreted from human body through the metabolic processes of the liver and kidneys. When diseases occur in the liver and kidneys, metabolic disorders cause higher ammonia levels in the body [1–3]. However, current medical measurement regarding ammonia levels in human body relies on blood analysis that is an invasive diagnostic with the risk of infection. In fact, ammonia can enter alveoli via passive diffusion and then is exhaled. The breath analysis for exhaled ammonia can be used for the identification and monitoring of procedures for clinical diagnostics due to the fact that the correlation between blood ammonia and breath ammonia has been verified [4].

At present, trace ammonia detection is demanded in various fields and a variety of detection methods were reported. In 2016, Andreas et al. [5] completed the detection of ammonia based on the chemo-resistive method. In 90% relative humidity, the detection sensitivity reaches 400 ppb. In 2021, Shao et al. [6] realized the detection of ammonia based on multi-walled carbon nanotube technology. The detection sensitivity reached 200 ppb, and the response time and recovery time were 17 s and 18 s, respectively. In 2014, Yao et al. [7] reported an ammonia sensor based on graphene/microfiber hybrid waveguide technology with a resolution of 300 ppb. Although all these methods enable the ammonia measurements, there is an urgent need for developing new ways to accomplish the detection of respiratory ammonia in humans owing to the requirements of extremely high resolution, small sample volume, rapid response time, and long calibration interval in respiratory analysis for clinical diagnostics.

In recent years, with the development of photoacoustic technology, more and more photoacoustic gas sensing systems were reported, among which the trace-gas sensor based on quartz-enhanced photoacoustic spectroscopy (QEPAS) is a suitable candidate for respiratory analysis as it is featured as better immunity to environmental acoustic noise and stronger capability to analyze trace gas samples. Instead of conventional microphones, the QEPAS based sensor employs a quartz tuning fork (QTF) as a resonant acoustic transducer, which 'listen' to a weak acoustic wave generated when optical radiation interacts with a trace gas [8,9]. So far, the QEPAS technology has been widely used in environmental monitoring, industrial process control, as well as security and defense [10–26]. In 2011, Lewicki et al. realized real-time measurement of human exhaled ammonia based on QEPAS, in which a 10.34-μm

* Corresponding author at: State Key Laboratory of Quantum Optics and Quantum Optics Devices, Institute of Laser Spectroscopy, Shanxi University, Taiyuan 030006, China.
E-mail address: donglei@sxu.edu.cn (L. Dong).

https://doi.org/10.1016/j.snb.2022.131510
Received 25 November 2021; Received in revised form 31 December 2021; Accepted 29 January 2022
Available online 1 February 2022

distributed feedback quantum cascade laser (DFB-QCL) was employed using a 3*f* wavelength locking technique. The sensor system achieved a high detection sensitivity of 6 ppb [27]. But the inherent high-*Q* characteristic of the QTF makes it susceptible to the environmental parameters, including temperature, pressure, humidity as well as flow and requires a long time to accumulate weak acoustic energy, which results in a frequent calibration requirement and a slow response time. Furthermore, the use of the 3*f* wavelength locking technique locking the laser wavelength onto the absorption line made the system complex and fragile.

In 2017, Wu et al. [28] put forward beat-frequency quartz-enhanced photoacoustic spectroscopy (BF-QEPAS), which offers unique advantages over the conventional QEPAS in terms of response time and calibration interval. The basic concept of BF-QEPAS requires that the laser modulation frequency is detuned from the QTF resonant frequency in such a way that when the laser wavelength has a quick scan through the targeted absorption line, a beat frequency signal between two frequencies can be generated, based on which the resonance frequency and *Q*-factor of the QTF, as well as the trace gas concentration, can be rapidly obtained simultaneously. Hence, BF-QEPAS avoids the calibration process and wavelength-locking requirement and permits real-time monitoring of a targeted trace gas. In this work, for the first time, we develop a calibration-free mid-infrared (MIR) exhaled breath sensor for real-time ammonia measurements at ppb level using BF-QEPAS and a 10.359 μm mid-IR QCL, removing the technical defects of the conventional QEPAS breath sensors, in which the frequency and *Q*-factor of the QTF requires to be calibrated frequently. Compared with previous work [30,31], our MIR exhaled breath sensor benefits from BF-QEPAS, offering higher sensitivity, faster response time, and no calibration requirement.

2. Selection of absorption line and light source for ammonia detection

A strong targeted absorption line is particularly important for the detection of human exhaled ammonia since exhaled ammonia levels are between 0 and 1500 ppb in general for a healthy person, which requires a high detection sensitivity. According to the HITRAN database, the simulated ammonia absorption intensity between 1 μm and 20 μm is shown in Fig. 1. The NH_3 molecule has four fundamental vibrational modes (ν_1, ν_2, ν_3, ν_4), in which the ν_2 band and other hot bands ($2\nu_2$-ν_2) near 10 μm (1000 cm^{-1}) obviously have the strongest absorption. In such a wavelength region, the main spectral interference comes from H_2O and CO_2 which are the important components of exhaled air. Spectral simulations for exhaled breath between 965.0 cm^{-1} to 966 cm^{-1} at 130 Torr were performed using the HITRAN database with H_2O (5%), CO_2 (5%), and NH_3 (10 ppb), as shown in the inset of Fig. 1. The use of low pressure is to avoid the spectral overlaps from the pressure broadening. One free from H_2O interference potential NH_3 absorption line can be detected at 965.35 cm^{-1}. Although a weak CO_2 line overlaps with the NH_3 line, we assess that there will not have a significant spectral interference from the weak CO_2 line, due to the fact that the linewidths of the two lines are very different so that an appropriate modulation depth matching the NH_3 linewidth can just pick out the NH_3 line, and on the other hand the concentration level of NH_3 in exhaled breath is much greater than 10 ppb. Therefore, the absorption line located at 965.35 cm^{-1} was determined as the targeted line.

A continuous-wave (CW) DFB-QCL emitting at a center wavelength of 10.359 μm was employed as the light source (Ningbo Healthy Photo Technology, QC-Qube 200831-AC712), to target the selected ammonia absorption line. The output wavelength and the power of the QCL as a function of the driving current were recorded using a wavelength meter and a power meter, respectively, as shown in Fig. 2. The wavelength tuning range covers from 964.955 cm^{-1} to 966.873 cm^{-1}. The corresponding current and temperature tuning rates with regards to wavenumber are calculated to be 0.009 cm^{-1}/mA and 0.0377 cm^{-1}/°C, respectively. The horizontal dash grey line in Fig. 2 marks the position of the selection absorption line. Since a higher optical power can induce a stronger photoacoustic signal, the laser power should be set as high as possible. Considering the limitation of the maximum laser current at 550 mA according to the laser datasheet, a laser power of 48 mW was selected, corresponding to the driving current and temperature of 532 mA and 30 °C, respectively.

3. Design of sensor system

The schematic diagram of the sensor system is shown in Fig. 3(a). The sensor system consists of three parts, a respiratory sampling system, a photoacoustic sensing unit, and a control and data processing unit. The respiratory sampling system was designed to collect the exhaled breath and to regulate the gas pressure and flow, providing a suitable measurement environment for photoacoustic detection. After a human subject breathed into the mouthpiece, the content of CO_2 and the airway pressure were monitored by a CO_2 mainstream module (Zhejiang National Medical, C500) and a mini pressure meter (CFsensor, XGZP6847A), respectively. Two needle valves were installed upstream and downstream of the photoacoustic sensing unit, which worked together with a diaphragm pump providing negative pressure, to set the pressure and gas flow rate of the photoacoustic sensing unit. A pinhole-

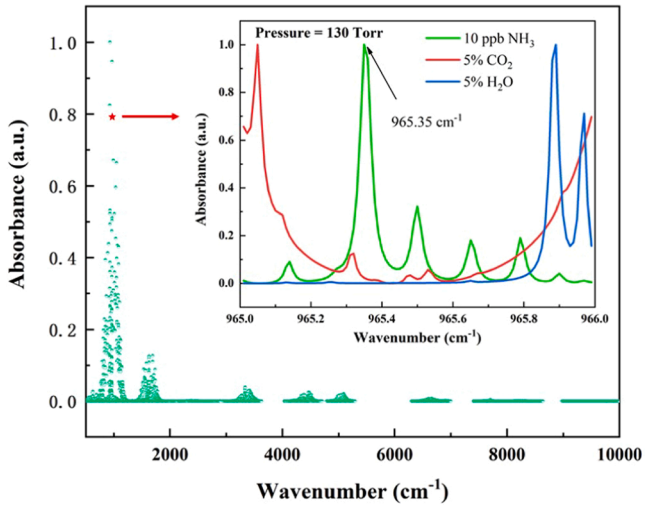

Fig. 1. Absorption lines of ammonia in the wavelength range of 1–20 μm. Inset: spectral simulation at 130 Torr with 10 ppb NH_3, 5% CO_2 and 5% H_2O.

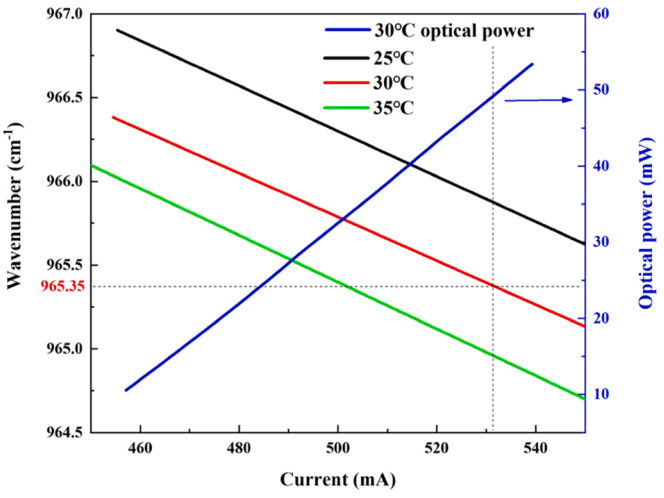

Fig. 2. QCL wavelengths as a function of current tuning at three (black, red, green lines) different operating temperatures. Blue line is the L-I curve at 30 °C.

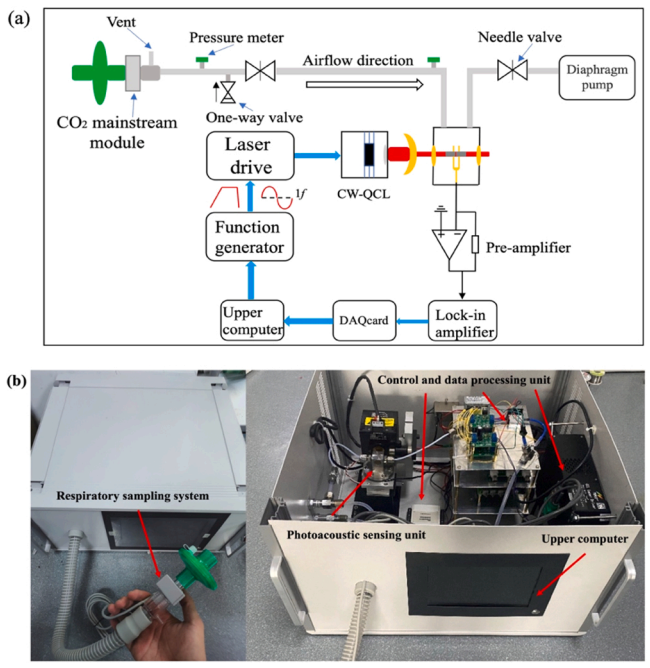

Fig. 3. (a) Schematic of human exhaled ammonia sensor based on BF-QEPAS; (b) prototype photos of human exhaled ammonia sensor based on BF-QEPAS.

sized vent was set after the CO_2 mainstream module to discharge the excess exhalation. A one-way valve was installed in front of the upstream valve, to quickly flush the photoacoustic sensing unit and thus to reset zero signal when stopping blowing.

The photoacoustic sensing unit is the core part of the sensor system, which used the BF-QEPAS technique and employed a small-sized piezoelectric QTF as an acoustic transducer. The QTF has a high resonance frequency of 2^{15} Hz (32,768 Hz) in a vacuum, resulting in immunity to low-frequency environmental noise for the photoacoustic measurement. The sound and vibration of the diaphragm pump does not affect QTF performance. Two acoustic micro-resonators with the lengths of 4.0 mm and the inner diameters of 0.8 mm were placed at two sides of the QTF, respectively, forming a spectrophone with an on-beam QEPAS configuration. Such a configuration can improve the signal-to-noise ratio up to 30 times [9]. The spectrophone was enclosed into a gas cell with two ZnSe windows, whose inlet and outlet were directed to the respiratory sampling system. The beam of the used DFB-QCL was focused by a ZnSe plane convex lens with a focal length of 25 mm and then passed through the acoustic micro resonators and the QTF in the gas cell. A low noise trans-impedance pre-amplifier with a feedback resistor of 10 MΩ was used to amplify the weak electrical signal from the QTF.

In the control and data processing unit, a laser driver (Healthy Photon QC750-Touch™) was employed, providing the operating current of the laser, and controlling its temperature. A commercial two-channel waveform generator circuit board (Juntek MHS5200A) produced a rapid scanning wave for the generation of the beat frequency signal and a sinusoidal wave for the wavelength modulation, both of which were added and then sent to the laser driver. The electrical signal from the QTF was demodulated by a lock-in amplifier board (FEMTO, LIV-BVD-150-H), then was collected by a 16-bit data acquisition card (DAQvantech, USB_HRF4626), and was finally processed by the LabVIEW program that ran on an upper computer. Two prototype photos of this sensor system regarding its appearance and internal structure are shown in Fig. 3(b).

Since ammonia is considered a polar molecule, it tends to stick to metal surfaces, delaying the response time and degrading the measurement accuracy. It is, therefore, important to understand the adsorption mechanism of ammonia on surfaces. The adsorption-desorption process under dynamic equilibrium can be expressed as [29]:

$$V\frac{\partial c_a^m}{\partial t} + c_a^m\Phi = c_a^{in}\Phi - \frac{\partial c_b}{\partial t}S \tag{1}$$

where V is the volume of the container [cm^3], c_a^m is the ammonia concentration [cm^{-3}] at the measurement point, Φ is the gas velocity [cm^3/s] in the gas path, c_a^{in} is the ammonia concentration at the gas path inlet, $\partial c_b/\partial t$ represents the effective adsorption rate [cm^{-2}/s] of ammonia molecules at quasi-steady state, S is the surface area of the gas cell [cm^2]. When $c_a^{in}\Phi \gg \frac{\partial c_b}{\partial t}S$, the inflow rate of ammonia molecules is much great than the adsorption rate and thus the viscous effect of the gas can be negligible. There are three ways to meet the above condition. First, since the ammonia concentration levels in exhaled breath are unpredictable, a higher gas flow rate Φ and a smaller surface area S are helpful to reduce the adsorption effect. Secondly, a higher temperature makes the ammonia molecules move quickly and reduces $\partial c_b/\partial t$. Thirdly a non-metallic material such as Teflon can provide a small $\partial c_b/\partial t$.

Based on the discussion about the adsorption-desorption effect, the piping in the respiratory sampling system was made of Teflon and was heated to 42 °C by means of a heating belt. In such a temperature, the adsorption effect of ammonia was reduced, the exhaled water vapor did not condense and the laser temperature can be easily controlled. The surface area of the gas cell is only 15 cm^2 thanks to the capability of QEPAS to analyze trace-gas samples. The gas flow rate was set to 60 sccm (standard cubic centimeter per minute), which is the maximum value that the respiratory sampling system can provide due to the capacity limit of the diaphragm pump operating at 130 Torr.

4. Self-calibration process

Compared with the conventional QEPAS, the BF-QEPAS has the advantage of being able to self-calibrate the QTF resonant frequency f_0 and quality factor Q. According to the beat frequency theory, f_0 can be expressed as [28]:

$$|f_0 \quad -f| = \quad \frac{1}{\Delta t} \quad = \Delta f \tag{2}$$

where f is the modulation frequency of the laser, Δt is the time difference between two adjacent peaks or valleys of the beat frequency signal and Δf is the difference between f_0 and f. Since f is known and Δt can be obtained from the beat frequency signal, f_0 can be derived from Eq. (2). According to the classical oscillator theory, the quality factor can be written as:

$$Q = \pi\tau f_0 \tag{3}$$

where τ is the response time of QTF which can be obtained from the decay time of the beat frequency signal. Thus, Q can also be calculated.

To prove the feasibility of this self-calibration approach, a certificated 1-ppm NH_3:N_2 gas mixture was filled into the sensor. A right-trapezoid-like waveform with a period of 330 ms was applied as the scanning waveform, corresponding to the laser current range of 525–538 mA and the wavenumber range of 965.45 cm^{-1} - 965.3 cm^{-1}. A 32.7 kHz sinusoidal waveform with a modulation depth of 0.047 cm^{-1} was used as the modulation signal. The integration time and the filter slope of the lock-in amplifier were set to 3 ms and 12 dB [28], respectively, corresponding to a detection bandwidth of 83.33 Hz to provide a sufficient response bandwidth and to maintain efficient background noise suppression. The beat frequency signal was demodulated at the 1 f mode. The measured beat frequency signal is shown in Fig. 4(a). The fluctuations of the beat frequency signal between 0 s and 0.05 s were from the neighboring ammonia line at 965.5 cm^{-1}. The time difference Δt between two adjacent peaks was measured to be 0.01887 s. The decay time τ was obtained to be 0.03778983 s through an exponential

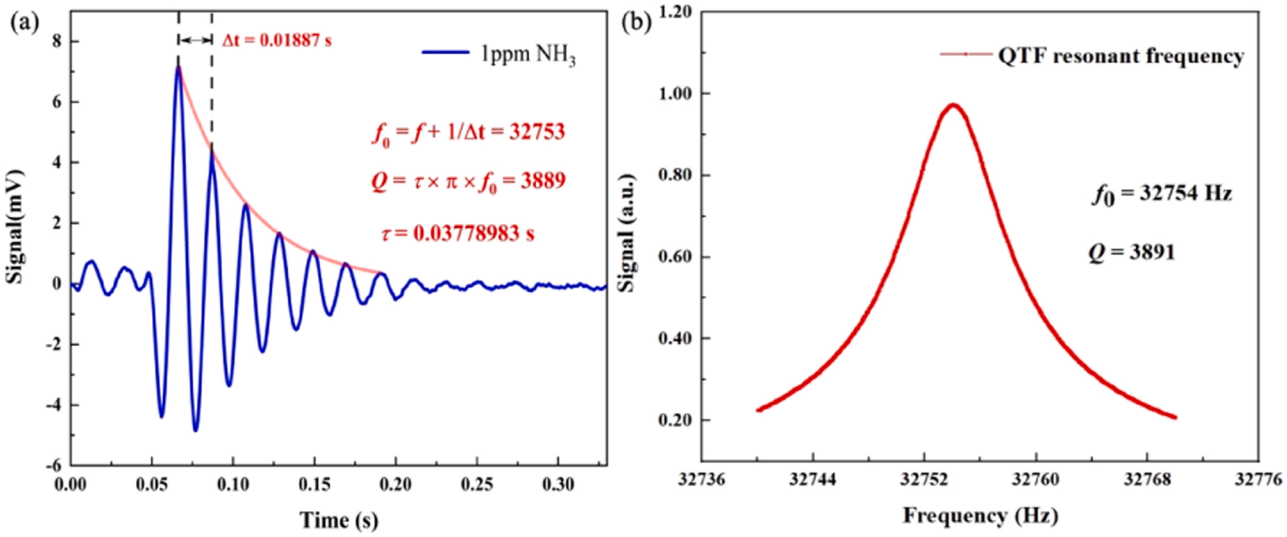

Fig. 4. (a) Beat frequency signal (blue line) from the sensing system. Decay time τ is derived by an exponential fitting (red line); (b) resonant curve of the QTF employed in the sensing system as a function of the vibration response of the electrical excitation.

fitting. Hence f_0 and Q can be calculated to be 32,753 Hz and 3889, respectively, according to Equ. (2)-(3). A traditional electric excitation method that must interrupt the process of gas concentration measurement was used to obtain the accurate f_0 and Q. The method gave $f_0 = 32,754$ Hz and $Q = 3891$. The good consistency between the results from the two methods verified the feasibility and reliability of the self-calibration approach. To maximize the detection sensitivity of the sensor system, the amplitude of the first maximum peak of the beat frequency signals was chosen as the signal value. A LabVIEW program was written and run in the upper computer to analyze the acquired beat frequency signal in real-time and self-calibrate the sensor system using the obtained f_0 and Q.

5. Experimental results and discussions

5.1. Modulation depth and frequency optimization

In conventional QEPAS-based sensors, the 1*f* signal amplitude is usually larger than the 2*f*'s. The reason why the 2*f* signal is usually adopted in the conventional QEPAS-based sensors is because the maximum value of the 2*f* signal corresponds to the peak of the measured absorption line. However, in BF-QEPAS, there is no difference between the waveforms of the 1*f* and 2*f* signals since an oscillating beat-frequency signal is measured. Thus, the 1*f* signal with a larger amplitude should be used to improve the detection sensitivity. The modulation depth was first optimized in the case of the 1-ppm NH_3:N_2 gas mixture filled into the gas cell. The amplitude of the first maximum peak of the beat frequency signals was acquired and depicted in Fig. 5 as a function of the modulation depth. The amplitude linearly increases together with the modulation depth increasing in the range of 0.004–0.025 cm^{-1}. Then the amplitude reaches the maximum value when the modulation depth is equal to 0.047 cm^{-1}, which is the optimal modulation depth.

The frequency difference Δf between f_0 and f is a very important parameter since the different Δf determines the different detection sensitivity. The amplitude of the first maximum peak of the beat frequency signal was recorded as a function of the modulation frequency f at the optimal modulation depth of 0.047 cm^{-1}, as shown in Fig. 6. The response curve of the QTF measured using the traditional electric excitation method is also plotted in Fig. 6. The maximum amplitude value of the conventional QEPAS 1*f* signals occurs at the resonant frequency f_0 of 32,754 Hz, while the local maximum amplitudes of the beat frequency

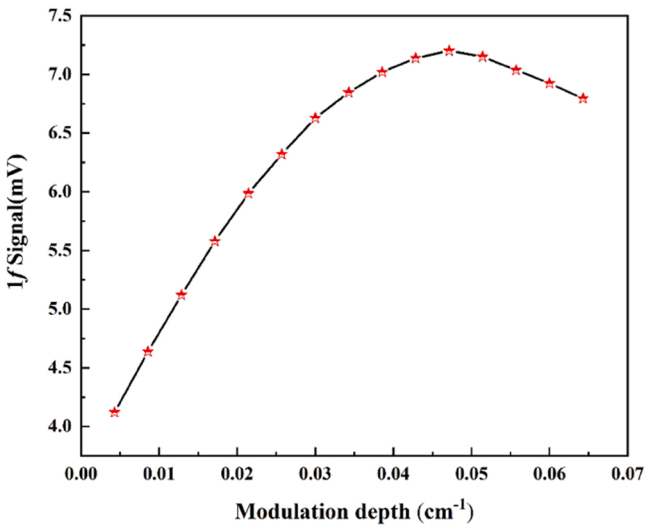

Fig. 5. Amplitude values of the beat frequency signal as a function of the modulation depths for a 1 ppm NH_3 at a pressure of 130 Torr.

signals occur at 32,704 Hz and 32,804 Hz, corresponding to a Δf of 50 Hz. Since f_0 is obtained in each measurement of the beat frequency signals, the new modulation frequency f can be calculated by Eq. (2), ensuring the consistency of the detection sensitivity once the QTF resonant frequency f_0 drifts.

5.2. Evaluation of sensor linearity

The linearity of the BF-QEPAS-based sensor system was assessed. The different concentration levels of NH_3, 50 ppb, 100 ppb, 200 ppb, 400 ppb, 600 ppb and 1 ppm, were generated by diluting the certificated 1 ppm NH_3:N_2 gas mixture using the gas dilution system and were directed into the sensing system in turn. 165 points were measured continuously for each concentration level with a data updating rate of 330 ms/point. High purity N_2 was introduced into the sensor for zero baseline measurement. Fig. 7(a) shows the experimental results. The amplitude of the beat frequency signals for 50 ppb NH_3 was 0.32 mV, while the standard deviation 1σ of the noise signal was 0.06089 mV, resulting in a signal-to-noise ratio of 5.25. The corresponding detection

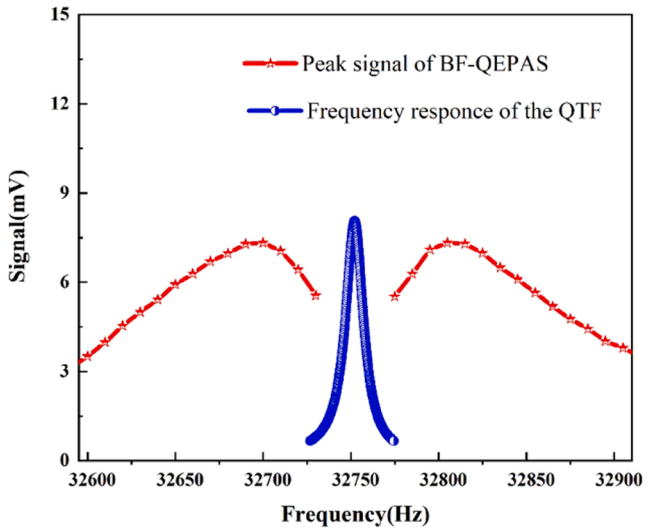

Fig. 6. Amplitudes of the beat-frequency (red line) and the conventional QEPAS (blue line) signals as a function of modulation frequency *f*.

limit and normalized noise equivalent absorption (NNEA) are 9.5 ppb and 1.42×10^{-9} cm^{-1} $W/Hz^{1/2}$, respectively. An average of the signal values was then performed for each concentration level, and the relationship as a function of concentration value was recorded in Fig. 7(b). The R-squared value between the measured and nominal concentrations was 0.999, confirming the good linear response of the sensor system to the NH_3 concentration.

6. Real-time ammonia measurement in exhaled human breath

Real-time ammonia measurement of exhaled human breath based on the BF-QEPAS sensor system was demonstrated. Eight healthy volunteers were asked to relax and complete the gent exhalation in a normal posture, as shown in Fig. 8(a). The subject does not need to make special preparatory movements before exhalation and try to empty the lungs of as much gas as possible during exhalation, making the measurements more accurate. The pressure values of the airway were displayed on the upper computer screen using a graduated bar so that the subjects can control their exhalation strength within the pressure range of 8–12 Torr according to the real-time pressure measurement. Such an exhalation control is to enable the subjects to have a continuous and stable blow and thus to maintain the stable pressure and flow rate of the sensor system.

The measurement result of one typical exhalation is presented in Fig. 8(b). The black line plus diamond represents the values of the airway pressure, which should be a horizontal line during an exhalation owing to the active pressure control. The blue line plus triangle represents the subject's exhaled CO_2 content, which is a real-time measurement of the reference profile for exhaled ammonia content. A healthy human exhales CO_2 at 4–6% at a time. And the CO_2 content should gradually rise with the blowing time, which can reflect the complete process of one exhalation. When any of the two curves are abnormal, it implies that a complete breathing process is not collected and the NH_3 data for this exhalation should be discarded. The red curve represents the NH_3 concentration values, which can be divided into four phases. Phase I is the rising process of the NH_3 signal. According to the airway pressure curve, the exhalation begins at 2 s, while the NH_3 concentration starts to rise at 3 s and ends at 10 s. The delay between the start of blowing and the maximum signal is partly because of the adsorption effect and partly because the exhaled breath needs to pass through a certain length of the tube to enter the gas cell. Subsequently, the concentration signal arrives in and stays a plateau, which is Phase II. However, this ammonia concentration does not come from the alveoli, but from the fermentation of residual food in the oral cavity since each subject has all kinds of food every day, and hence cannot be used as a valid test result. In Phase III, with the NH_3 in the oral cavity evacuated, the NH_3 concentration drops and then stays at a lower plateau, as shown in the cyan rectangle of Fig. 8(b). The measured value at this time, corresponding to 290ppb, reflects the true concentration level of NH_3 in the alveoli and can be used as a clinical reference. At the time of 32 s, the exhalation process enters Phase IV where the exhalation stops as the airway pressure drops to zero. The zeroing process of the NH_3 signal takes ~9 s (32–41 s) due to the adsorption effect, while the CO_2 signal quickly returns to zero. The measurement results of the eight healthy subjects are presented in Fig. 8(a), having a concentration distribution in the range of 150–640ppb, which are below the safety threshold of 1500 ppb. The result shows that even the healthy subjects have a large concentration differences between individuals.

7. Conclusions

An exhaled breath sensor for real-time ammonia measurements at ppb level was developed based on the BF-QEPAS technique. This sensor combined the main characteristics of QEPAS with the new benefits of BF-QEPAS, thus providing higher sensitivity, faster response time,

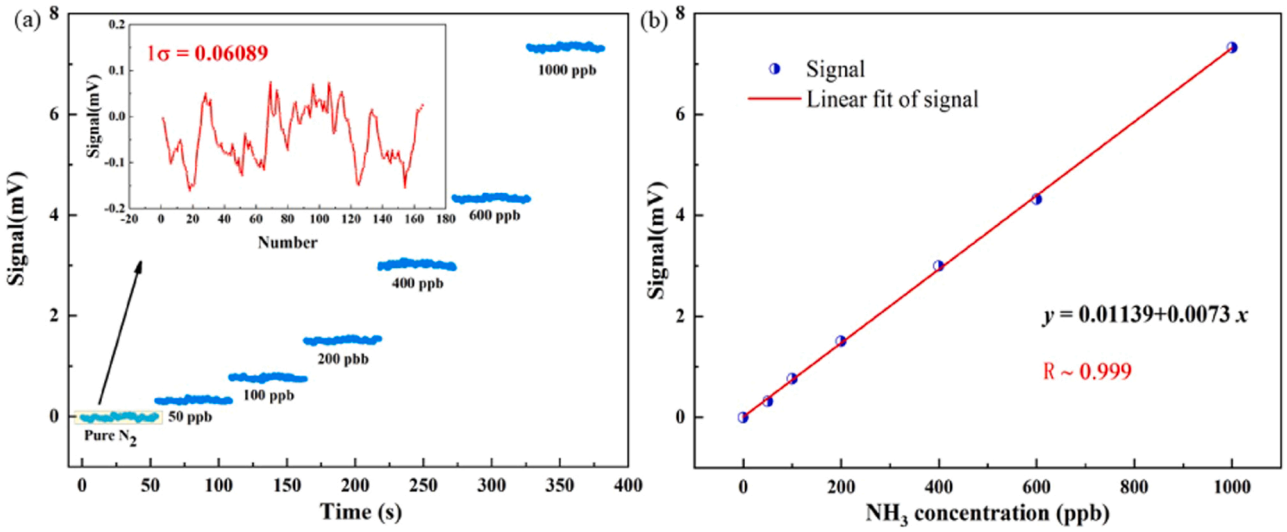

Fig. 7. (a) Beat-frequency signals generated by the sensor system at different concentration levels of ammonia; (b) linearity of the sensor system.

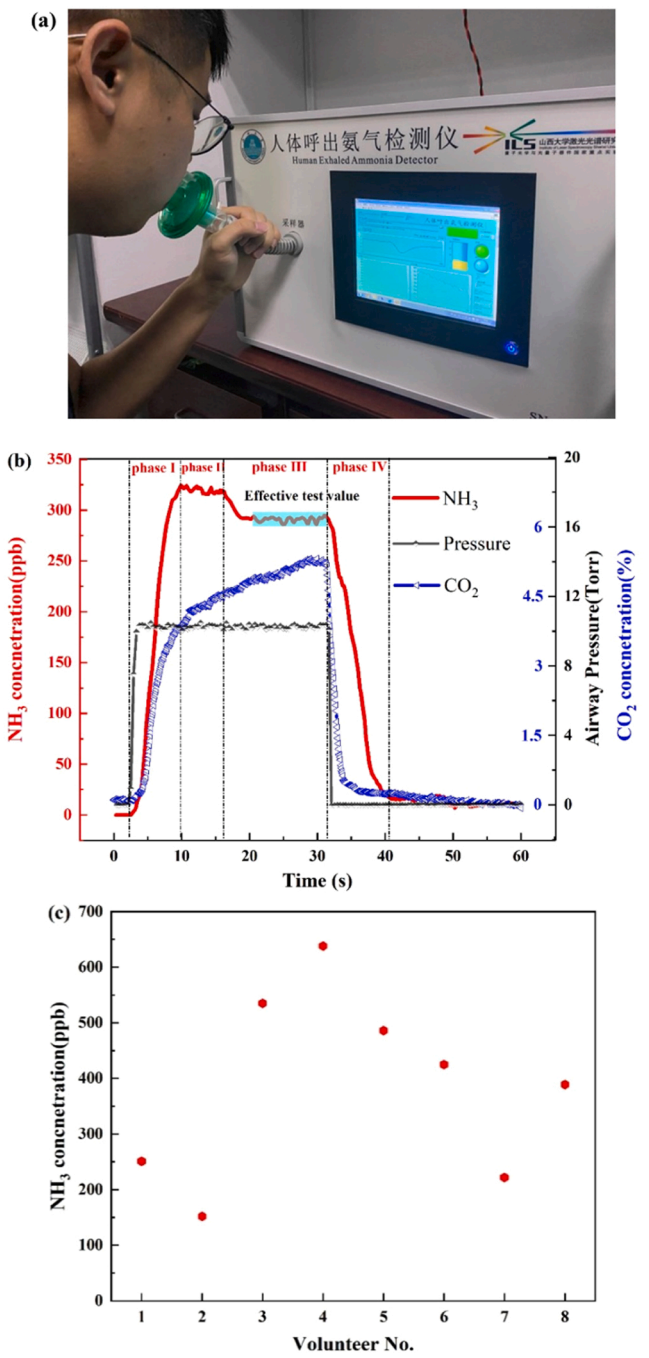

Fig. 8. (a) Volunteer test photo; (b) real-time measurement graph of a volunteer using BF-QEPAS. The red curve in the graph indicates the change in the exhaled ammonia level of the volunteer during one measurement, the black curve indicates the change in the airway pressure during one measurement, and the blue curve indicates the change in the exhaled CO_2 level of the volunteer during one measurement; (c) exhaled ammonia levels of 8 tested healthy volunteers.

capability to analyze trace gas samples, as well as no need for calibration and wavelength locking. The detection sensitivity of 9.5 ppb was achieved at a 3-ms integration time, corresponding to a NNEA of 1.42×10^{-9} cm^{-1} $W/Hz^{1/2}$. The identification and quantification of breath ammonia can be used as a clinical reference for the non-invasive diagnosis of liver and kidney diseases. The possibility of real-time calibration-free testing for diseases in a non-invasive manner, without the need for chemical reagents and complex professional laboratory facilities, is particularly appealing in view of the current global pandemic. Deployment of the sensor system in hospitals for field tests of the patients with liver and kidney disease to evaluate its performance will be conducted in the coming future.

CRediT authorship contribution statement

Biao Li: Writing – original draft, Investigation. **Chaofan Feng:** Software, Validation, Data curation. **Hongpeng Wu:** Visualization, Project administration. **Suotang Jia:** Methodology. **Lei Dong:** Conceptualization, Supervision, Writing – review & editing.

Declaration of Competing Interest

The authors declare that they have no known competing financial interests or personal relationships that could have appeared to influence the work reported in this paper.

Acknowledgements

The project is sponsored by National Key R&D Program of China (No. 2019YFE0118200); National Natural Science Foundation of China (NSFC) (Nos. 62175137, 62075119 and 61805132); Sanjin Scholar (No. 2017QNSJXZ-04), and Shanxi "1331KSC".

References

[1] L.A. Spacek, A. Strzepka, S. Saha, J. Kotula, J. Gelb, S. Guilmain, T. Risby, S. F. Solga, Repeated measures of blood and breath ammonia in response to control, moderate and high protein dose in healthy men, Sci. Rep. 8 (2018) 2554, https://doi.org/10.1038/s41598-018-20503-0.

[2] L.A. Spacek, M. Mudalel, F. Tittel, T.H. Risby, S.F. Solga, Clinical utility of breath ammonia for evaluation of ammonia physiology in healthy and cirrhotic adults, J. Breath Res. 9 (2015), 047109, https://doi.org/10.1088/1752-7155/9/4/047109.

[3] B. Timmer, W. Olthuis, A. van den Berg, Ammonia sensors and their applications - a review, Sens. Actuators B: Chem. 107 (2) (2005) 666–677, https://doi.org/10.1016/j.snb.2004.11.054.

[4] L.R. Narasimhan, W. Goodman, C. Kumar, N. Patel, Correlation of breath ammonia with blood urea nitrogen and creatinine during hemodialysis, PNAS 98 (8) (2001) 4617–4621.

[5] A.T. Güntner, M. Righettoni, S.E. Pratsinis, Selective sensing of NH_3 by Si-doped α-MoO_3 for breath analysis, Sens. Actuators B: Chem. 223 (2016) 266–273, https://doi.org/10.1016/j.snb.2015.09.094.

[6] S. Shao, C. Xie, L. Zhang, S. Wei, H.W. Kim, S.S. Kim, CsPbI3NC-sensitized SnO_2/Multiple-walled carbon nanotube self-assembled nanomaterials with highly selective and sensitive NH_3 sensing performance at room temperature, ACS Appl. Mater. Interfaces 13 (12) (2021) 14447–14457, https://doi.org/10.1021/acsami.0c20566.

[7] B. Yao, Y. Wu, Y. Cheng, A. Zhang, Y. Gong, Y.J. Rao, Z. Wang, Y. Chen, All-optical Mach-Zehnder interferometric NH_3 gas sensor based on graphene/microfiber hybrid waveguide, Sens. Actuators B: Chem. 194 (2014) 142–148, https://doi.org/10.1016/j.snb.2013.12.085.

[8] A.A. Kosterev, Y.A. Bakhirkin, R.F. Curl, F.K. Tittel, Quartz-enhanced photoacoustic spectroscopy, Opt. Lett. 27 (21) (2002) 1902–1904, https://doi.org/10.1364/OL.27.001902.

[9] L. Dong, A.A. Kosterev, D. Thomazy, F.K. Tittel, QEPAS spectrophones: design, optimization, and performance, Appl. Phys. B: Lasers Opt. 100 (3) (2010) 627–635, https://doi.org/10.1007/s00340-010-4072-0.

[10] Y. Ma, R. Lewicki, M. Razeghi, F.K. Tittel, QEPAS based ppb-level detection of CO and N2O using a high power CW DFB-QCL, Optics Exp. 21 (1) (2013) 1008–1019, https://doi.org/10.1364/OE.21.001008.

[11] K. Liu, X. Guo, H. Yi, W. Chen, W. Zhang, X. Gao, Off-beam quartz-enhanced photoacoustic spectroscopy, Opt. Lett. 34 (10) (2009) 1594–1596, https://doi.org/10.1364/OL.34.001594.

[12] S. Borri, P. Patimisco, A. Sampaolo, H.E. Beere, D.A. Ritchie, M.S. Vitiello, G. Scamarcio, V. Spagnolo, Terahertz quartz enhanced photo-acoustic sensor, Appl. Phys. Lett. 103 (2013), https://doi.org/10.1063/1.4812438 (021105-87).

[13] K. Chen, B. Zhang, M. Guo, Y. Chen, H. Deng, B. Yang, S. Liu, F. Ma, F. Zhu, Z. Gong, Q. Yu, Photoacoustic trace gas detection of ethylene in high-concentration methane background based on dual light sources and fiber-optic microphone, Sens. Actuators B: Chem. 310 (2020), 127825, https://doi.org/10.1016/j.snb.2020.127825.

[14] V. Spagnolo, P. Patimisco, S. Borri, G. Scamarcio, B.E. Bernacki, J. Kriesel, Part-per-trillion level SF_6 detection using a quartz enhanced photoacoustic spectroscopy-based sensor with single-mode fiber-coupled quantum cascade laser excitation. Opt. Lett. 37 (21) (2012) 4461–4463, https://doi.org/10.1364/OL.37.004461.

[15] P. Patimisco, A. Sampaolo, L. Dong, F.K. Tittel, V. Spagnolo, Recent advances in quartz enhanced photoacoustic sensing, Appl. Phys. Rev. 5 (2018), 011106, https://doi.org/10.1063/1.5013612.
[16] M.W. Sigrist, Mid-infrared laser-spectroscopic sensing of chemical species, J. Adv. Res. 6 (3) (2015) 529–533, https://doi.org/10.1016/j.jare.2014.09.002.
[17] W. Ren, A. Farooq, D.F. Davidson, R.K. Hanson, CO concentration and temperature sensor for combustion gases using quantum-cascade laser absorption near 4.7 μm, Appl. Phys. B: Lasers Opt. 107 (3) (2012) 849–860, https://doi.org/10.1007/s00340-012-5046-1.
[18] K. Zheng, C. Zheng, N. Ma, Z. Liu, Y. Yang, Y. Zhang, Y. Wang, F.K. Tittel, Near-infrared broadband cavity-enhanced spectroscopic multigas sensor using a 1650 nm light emitting diode, ACS Sens. 4 (7) (2019) 1899–1908, https://doi.org/10.1021/acssensors.9b00788.
[19] J. Hayden, B. Baumgartner, J.P. Waclawek, B. Lendl, Mid-infrared sensing of CO at saturated absorption conditions using intracavity quartz-enhanced photoacoustic spectroscopy, Appl. Phys. B: Lasers Opt. 125 (2019) 159, https://doi.org/10.1007/s00340-019-7260-6.
[20] H. Zheng, Y. Liu, H. Lin, B. Liu, X. Gu, D. Li, B. Huang, Y. Wu, L. Dong, W. Zhu, J. Tang, H. Guan, H. Lu, Y. Zhong, J. Fang, Y. Luo, J. Zhang, J. Yu, Z. Chen, F. K. Tittel, Quartz-enhanced photoacoustic spectroscopy employing pilot line manufactured custom tuning forks, Photoacoustics 17 (2020), 100158, https://doi.org/10.1016/j.pacs.2019.100158.
[21] H. Wu, L. Dong, X. Yin, A. Sampaolo, P. Patimisco, W. Ma, L. Zhang, W. Yin, L. Xiao, V. Spagnolo, S. Jia, Atmospheric CH_4 measurement near a landfill using an ICL-based QEPAS sensor with V-T relaxation self-calibration, Sens. Actuators B: Chem. 297 (2019), 126753, https://doi.org/10.1016/j.snb.2019.126753.
[22] A. Sampaolo, C. Yu, T. Wei, A. Zifarelli, M. Giglio, P. Patimisco, H. Zhu, H. Zhu, L. He, H. Wu, L. Dong, G. Xu, V. Spagnolo, H_2S quartz-enhanced photoacoustic spectroscopy sensor employing a liquid-nitrogen-cooled THz quantum cascade laser operating in pulsed mode, Photoacoustics 21 (2021), 100219, https://doi.org/10.1016/j.pacs.2020.100219.
[23] T. Wei, A. Zifarelli, S. dello Russo, H. Wu, G. Menduni, P. Patimisco, A. Sampaolo, V. Spagnolo, L. Dong, High and flat spectral responsivity of quartz tuning fork used as infrared photodetector in tunable diode laser spectroscopy, Appl. Phys. Rev. 8 (2021), 041409, https://doi.org/10.1063/5.0062415.
[24] H. Lv, H. Zheng, Y. Liu, Z. Yang, Q. Wu, H. Lin, Z.A.B. Montano, W. Zhu, J. Yu, R. Kan, Z. Chen, F.K. Tittel, Radial-cavity quartz-enhanced photoacoustic spectroscopy, Opt. Lett. 46 (16) (2021) 3917–3920, https://doi.org/10.1364/OL.432308.
[25] W. Trzpil, J. Charensol, D. Ayache, N. Maurin, R. Rousseau, A. Vicet, M. Bahriz, A silicon micromechanical resonator with capacitive transduction for enhanced photoacoustic spectroscopy, Sens. Actuators B: Chem. 353 (2021), 131070, https://doi.org/10.1016/j.snb.2021.131070.
[26] Z. Wang, Q. Wang, J.Y. Ching, J.C. Wu, G. Zhang, W. Ren, A portable low-power QEPAS-based CO_2 isotope sensor using a fiber-coupled interband cascade laser, Sens. Actuators B: Chem. 246 (2017) 710–715, https://doi.org/10.1016/j.snb.2017.02.133.
[27] R. Lewicki, A.A. Kosterev, D.M. Thomazy, T.H. Risby, S. Solga, T.B. Schwartz, F. K. Tittel, Real time ammonia detection in exhaled human breath using a distributed feedback quantum cascade laser based sensor, Quantum Sens. Nanophotonic Dev. VIII 79450K (2011) 79450K, https://doi.org/10.1117/12.874887.
[28] H. Wu, L. Dong, H. Zheng, Y. Yu, W. Ma, L. Zhang, W. Yin, L. Xiao, S. Jia, F. K. Tittel, Beat frequency quartz-enhanced photoacoustic spectroscopy for fast and calibration-free continuous trace-gas monitoring, Nat. Commun. 8 (2017) 15331, https://doi.org/10.1038/ncomms15331.
[29] A. Schmohl, A. Miklos, P. Hess, Effects of adsorption-desorption processes on the response time and accuracy of photoacoustic detection of ammonia, Appl. Opt. 40 (15) (2001) 2571–2578, https://doi.org/10.1364/AO.40.002571.
[30] J. Wang, W. Zhang, L. Li, Q. Yu, Breath ammonia detection based on tunable fiber laser photoacoustic spectroscopy, Appl. Phys. B: Lasers Opt. 103 (2) (2011) 263–269, https://doi.org/10.1007/s00340-011-4550-z.
[31] J. Manne, O. Sukhorukov, W. Jäger, J. Tulip, Pulsed quantum cascade laser-based cavity ring-down spectroscopy for ammonia detection in breath, Appl. Opt. 45 (36) (2006) 9230–9237, https://doi.org/10.1364/AO.45.009230.

Biao Li is now pursuing a Ph.D. degree in atomic and molecular physics in the Institute of Laser Spectroscopy of Shanxi University, China. His research interests include gas sensors, photoacoustic spectroscopy, and laser spectroscopy techniques.

Chaofan Feng is now pursuing a Ph.D. degree in atomic and molecular physics in the Institute of Laser Spectroscopy of Shanxi University, China. His research interests include gas sensors, photoacoustic spectroscopy, and laser spectroscopy techniques.

Hongpeng Wu received his Ph.D. degree in atomic and molecular physics from Shanxi University, China, in 2017. From 2015 to 2016, he studied as a joint Ph.D. student in the electrical and computer engineering department and rice Quantum Institute, Rice University, Houston, USA. Currently, he is a professor at the Institute of Laser Spectroscopy of Shanxi University. His research interests include optical sensors and laser spectroscopy techniques.

Suotang Jia received his B.S. degree in physics in 1986 and the M.S. degree in optics in 1989 from Shanxi University, China. He graduated in 1994 with a Ph.D. degree from the East China Normal University. Since 1996, he has worked as a visiting scholar at the CNRS in France, the University of Maryland, Yale University and University of Connecticut. He is now a professor at Shanxi University and became President of Shanxi University in 2012. His research interests include quantum optics, quantum information, ultracold atom and molecules as well as applications of laser spectroscopy.

Lei Dong received his Ph.D. degree in optics from Shanxi University, China, in 2007. From June 2008 to December 2011, he worked as a post-doctoral fellow in the Electrical and Computer Engineering Department and Rice Quantum Institute, Rice University, Houston, USA. Currently, he is a professor in the Institute of Laser Spectroscopy of Shanxi University. His research activities are focused on research and development in laser spectroscopy, in particular photoacoustic spectroscopy applied to sensitive, selective, and real-time trace gas detection, and laser applications in environmental monitoring, chemical analysis, industrial process control, and medical diagnostics. He has published more than 100 peer-reviewed papers with $>$ 2200 positive citations.